RESEARCH ARTICLE | DECEMBER 19 2023

SQUID-based superconducting microcalorimeter with *in situ* tunable gain

C. Schuster ✉ iD ; S. Kempf iD

Check for updates

View Online   Export Citation

Articles You May Be Interested In

A high resolution gamma-ray spectrometer based on superconducting microcalorimeters

Rev. Sci. Instrum. (September 2012)

Anomalous Thermal Behavior in Microcalorimeter Gamma-Ray Detectors

AIP Conf. Proc. (December 2009)

Code-division-multiplexed readout of large arrays of TES microcalorimeters

Appl. Phys. Lett. (September 2016)

SQUID-based superconducting microcalorimeter with *in situ* tunable gain

View Online   Export Citation   CrossMark

C. Schuster[1,a)] (ID) and S. Kempf[1,2] (ID)

AFFILIATIONS

[1]Institute of Micro- and Nanoelectronic Systems, Karlsruhe Institute of Technology, Hertzstrasse 16, Building 06.41,
 D-76187 Karlsruhe, Germany
[2]Institute for Data Processing and Electronics, Karlsruhe Institute of Technology, Hermann-von-Helmholtz-Platz 1,
 Building 242, D-76344 Eggenstein-Leopoldshafen, Germany

[a)]Author to whom correspondence should be addressed: constantin.schuster@kit.edu

ABSTRACT

Cryogenic microcalorimeters are outstanding tools for x-ray spectroscopy due to their unique combination of excellent energy resolution and close to 100% detection efficiency. While well-established microcalorimeter concepts have already proven impressive performance, their energy resolution has yet to improve to be competitive with cutting-edge wavelength-dispersive grating or crystal spectrometers. We hence present an innovative SQUID-based superconducting microcalorimeter with an *in situ* tunable gain as alternative concept that is based on the strong temperature dependence of the magnetic penetration depth of a superconductor operated close to its critical temperature. Measurements using a prototype device show no sign for any hysteresis effects that often spoil the performance of superconducting microcalorimeters. Moreover, our predictions of the achievable energy resolution show that a competitive energy resolution $\mathcal{O}(300\,\text{meV})$ with a suitable combination of absorber and sensor material should be easily possible.

Cryogenic microcalorimeters such as superconducting transition-edge sensors (TESs)[1,2] or metallic magnetic calorimeters (MMCs)[3,4] have proven to be outstanding devices to measure the energy of x-ray photons with utmost precision. They rely on sensing the change in temperature of an x-ray absorber upon photon absorption using an extremely sensitive thermometer that is based on either a superconducting (TES) or a paramagnetic (MMC) sensor material. Thanks to their exceptional combination of an outstanding energy resolution and a quantum efficiency close to 100%, they are highly attractive for x-ray emission spectroscopy (XES), both at synchrotron light sources and in a laboratory environment.[5,6] They strongly relax the requirements on x-ray beam intensity as compared to state-of-the-art wavelength-dispersive x-ray spectrometers based on diffraction gratings or bent crystals.[7] Moreover, they cover the entire tender x-ray range[7] that is hardly accessible with both, grating and crystal spectrometers, and allow studying strongly diluted as well as radiation-sensitive samples that can, even at the most brilliant synchrotron light sources, only be investigated with greatest efforts.[5,6]

Current cutting-edge TES- and MMC-based detectors achieve an energy resolution ΔE_{FWHM} of 0.72 eV for 1.5 keV photons[8] and of

1.25 eV for 5.9 keV photons[9] and provide a quantum efficiency close to 100% in this energy range. In terms of resolution, they come close to the resolution of wavelength-dispersive x-ray spectrometers while offering orders of magnitude higher efficiency. However, despite this great success, both detector types face some challenges that presently prevents these detectors from reaching an energy resolution in the range of 100 meV as required for investigating vibrations or *d-d*-excitations in soft x-ray spectroscopy or resonant inelastic x-ray scattering. It might hence be worthwhile to look for alternate detector concepts in addition to advancing the present leading technologies.

Here, we present an innovative SQUID-based microcalorimeter with *in situ* tunable gain that appears to be particularly suited for high-resolution soft x-ray spectroscopy. It is based on the strong temperature dependence of the magnetic penetration depth $\lambda(T)$ of a superconducting material that is operated close to its critical temperature T_c. Figure 1 depicts a simplified schematic circuit diagram of our microcalorimeter, which we denote as λ-SQUID. It largely resembles a conventional low-T_c dc-SQUID that comprises two identical resistively shunted Josephson tunnel junctions with critical current I_c and normal state resistance R as well as a closed superconducting loop formed by
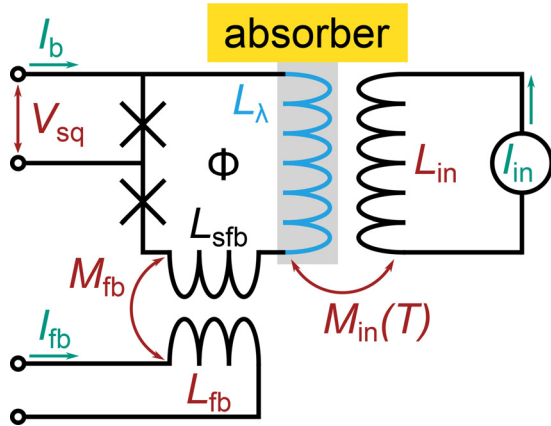
FIG. 1. Schematic circuit diagram of a λ-SQUID. Inductors depicted in black are made from a superconducting material with critical temperature T_c. The λ-coil displayed in blue is made from a different superconducting material with critical temperature $T_c^\lambda \ll T_c$ and is in strong thermal contact with the absorber. The device is operated at temperature $T_0 \lesssim T_c^\lambda$. A current source runs a constant current I_{in} through an input coil with inductance L_{in}. The λ-coil and the input coil are inductively coupled via the mutual inductance $M_{in}(T)$ that is temperature-dependent because of the temperature dependence of the magnetic penetration depth $\lambda(T)$ of the λ-coil.

two inductors with inductances L_λ and L_{sfb}, respectively. The Josephson junctions, the inductor L_{sfb} as well as the superconducting wiring are made from a superconducting material with critical temperature $T_c \gg T_0$ that is much greater than the operating temperature T_0 of the microcalorimeter. In contrast, the inductor L_λ, which we will refer to as λ-coil is made from a superconducting material with much lower critical temperature $T_c^\lambda \gtrsim T_0$ that exceeds only barely the device operating temperature T_0. It is worth mentioning that for a practical device, the operation temperature will be chosen according to the transition temperature of the λ-coil, and not vice versa. The λ-coil is coupled to the input coil with inductance L_{in} via the mutual inductance $M_{in} = k\sqrt{L_\lambda L_{in}}$. Here, k denotes the magnetic coupling factor. Since the λ-coil is operated near its critical temperature, its magnetic penetration depth $\lambda(T)$ depicts a strong temperature dependence, resulting in a temperature dependence of its inductance $L_\lambda(T) = L_{\lambda,geo}(T) + L_{\lambda,kin}(T)$. Here, $L_{\lambda,geo}(T)$ and $L_{\lambda,kin}(T)$ represent the geometric and kinetic contributions to the total coil inductance. The magnetic penetration depth influences the geometric inductance $L_{\lambda,geo}(T)$ via the distribution of current density in the cross section of the inductor, which ultimately causes a temperature dependence of the mutual inductance $M_{in}(T)$.

The device is biased either with a constant current I_b, with the resulting voltage drop V_{SQ} across the device being used as output signal, or with a constant voltage V_b, the current I_{SQ} running through the devices acting as output signal. In any case, the output signal depends on the total magnetic flux Φ_{tot} threading the SQUID loop. A current source supplying a constant current I_{in} is connected to the input coil. This current induces a magnetic flux $\Phi(T) = M_{in}(T)I_{in}$ within the SQUID loop that is temperature dependent via the temperature dependence of the mutual inductance $M_{in}(T)$.

By attaching a suitable x-ray absorber to the λ-coil, the absorption of an x-ray photon causes a temperature rise of this coil that is

transduced into a change of magnetic flux within the SQUID loop. The latter can be sensed as a change of output signal. An additional coil with inductance L_{fb} is inductively coupled to the λ-SQUID via the inductor L_{sfb} and mutual inductance M_{fb}. This coil allows for additional control of the magnetic flux threading the SQUID loop by running an externally controlled current I_{fb} through it.

For the following discussion, we assume a constant current bias. In this case, the relationship between output signal voltage V_{SQ} and temperature T is defined by the gain coefficient

$$\frac{\partial V_{SQ}}{\partial T} = \frac{\partial V_{SQ}}{\partial \Phi}\frac{\partial M_{in}}{\partial T}I_{in}, \qquad (1)$$

where the flux-to-voltage transfer coefficient can be estimated by $\partial V_{SQ}/\partial \Phi = R/L_{SQ}$ for an optimized dc-SQUID.[10] Here, L_{SQ} denotes the total SQUID inductance. From Eq. (1), the tunability of the gain factor gets clearly apparent: with I_{in} being limited solely by the ampacity of the input coil and the temperature dependence $\partial M_{in}/\partial T$ depending on the operation temperature, the gain coefficient can be varied by both, the input current and operation temperature, over a wide range. Moreover, with a sufficient choice of the current I_{in}, the gain coefficient can be made suitably large, even if $\partial M_{in}/\partial T$ itself is rather small. In addition, as the current I_{in} can be changed fast, e.g., by external control electronics, the gain can be even tuned *in situ*, i.e., even during the acquisition of a detection event. This enables additional degrees of freedom during readout, e.g., by ensuring that the dynamic range of analog to digital converters in the readout chain is always fully utilized.

We fabricated a prototype device that is depicted in Fig. 2(a). It is based on the design of one of our custom-made dc-SQUIDs for MMC readout and features four superconducting loops that are connected in parallel [Fig. 2(b)]. Each loop is inductively coupled to a flux biasing as well as an input coil where the coil arrangement is engineered such that the mutual inductance between these coils is greatly reduced. The majority of the device including the actual input coil with inductance L_{in} and flux biasing coil with inductance L_{fb} is fabricated from niobium having a critical temperature $T_c \simeq 8.9$ K. The part of the SQUID loop that is coupled to the input coil acts as λ-coil and is made from aluminum with critical temperature $T_c^\lambda \simeq 1.2$ K. We note that aluminum is an unfavorable sensor material for a real microcalorimeter (as the thermal noise at $\simeq 1.2$ K would prevent to reach an energy resolution in the range of 1 eV or below). However, this choice was triggered by our intention to use this device only for proving the suitability of our microcalorimeter concept and to estimate its sensitivity as well as the fact that an easy-to-deposit elemental superconductor with T_c in the range of $50-100$ mK does not exist. We consequently postponed the development of a sophisticated deposition process for a superconducting material with suitable T_c and also omitted the particle absorber. A full working microcalorimeter comprising a low T_c material for the λ-coil as well as a suitable x-ray absorber will hence be the subject of future work.

We comprehensively characterized our prototype device in a ^{3}He/^{4}He dilution refrigerator that was tweaked to smoothly run up to temperatures of about 1.5 K. We used a resistive heater mounted at the mixing-chamber platform to control the operation temperature and bias and read out the detector using a direct-coupled high-speed dc-SQUID electronics.[11] Figure 3(a) shows the measured output voltage V_{SQ} across the device vs the applied input current I_{in} at two
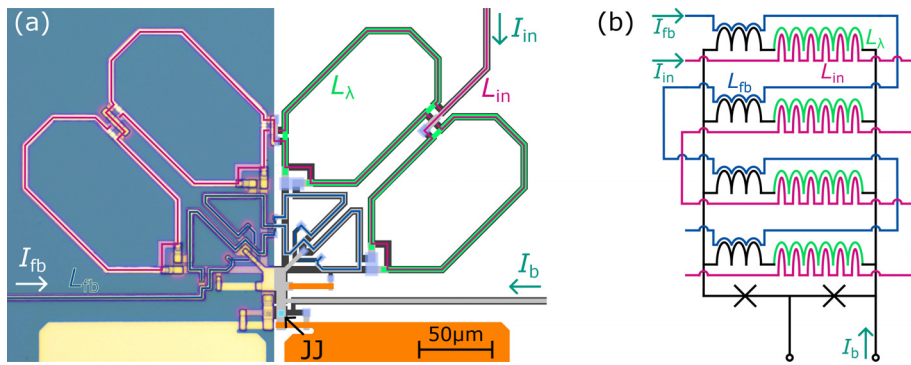
FIG. 2. (a) Micrograph (left) and design layout (right) as well as (b) equivalent circuit diagram of our prototype λ-SQUID. The λ-coil (green in the design and circuit diagram, bright yellow in the micrograph) is made from Al ($T_c^\lambda \simeq 1.2\,\mathrm{K}$), while the other parts of the device are made from Nb ($T_c \simeq 8.9\,\mathrm{K}$). In (a), the paths of the input and flux biasing coils are traced in magenta and blue, respectively.

different operating temperatures T_0 close to the critical temperature T_c^λ of the λ-coil. The periodic response of dc-SQUIDs is clearly visible. For small input currents, the tiny temperature-induced change of the mutual inductance hardly creates a measured voltage change ΔV_{SQ}. However, the larger the I_{in}, the larger was the ΔV_{SQ}. This directly resembles the prediction according to Eq. (1) and proves the *in situ* tunability of the gain factor. In Fig. 3(b), the gain coefficient $\partial V_{\mathrm{SQ}}/\partial T$ is depicted vs both the input current I_{in} and the reduced operation temperature $\tilde{t}_0 = T_0/T_c^\lambda$, illustrating the large tuning range available with these two parameters.

To determine the temperature dependence of the mutual inductance $M_{\mathrm{in}}(T)$ as well as the sensitivity coefficient $\partial V_{\mathrm{SQ}}/\partial T$, we performed two different types of measurements: For static measurements, we injected a linear current ramp into the input coil and monitored the output voltage V_{SQ}. The current change ΔI_{in} for a flux change of a single flux quantum Φ_0 then allows to determine the mutual inductance via $M_{\mathrm{in}} = \Phi_0/\Delta I_{\mathrm{in}}$. For flux ramp modulated [12,13] (FRM) measurements, we injected a constant input current I_{in} into the input coil and applied a periodic sawtooth-like current ramp with amplitude I_{ramp} and repetition rate f_{ramp} to the flux biasing coil. We chose the ramp amplitude I_{ramp} such that in each cycle an integer multiple of flux quanta was induced into the λ-SQUID. In this mode of operation, the output voltage V_{SQ} is modulated with a well-defined frequency. Any flux signal Φ that is quasi-static with respect to the ramp repetition rate f_{ramp} is then transduced into a phase shift $\Theta = 2\pi\Phi/\Phi_0$ of the periodic output voltage V_{SQ}. The flux contribution $\Phi(T) = M_{\mathrm{in}}(T)I_{\mathrm{in}}$ resulting from the constant current within the

input coil changes with temperature and can be derived from the phase shift $\Theta(T)$ of the λ-SQUID response. The latter can be determined by demodulation of the SQUID output voltage. It is worth mentioning that a change in the SQUID output voltage can be caused by a shift of the working point, too, and may affect the shape and offset of the periodic output voltage. However, the FRM phase and thus demodulated flux signal remain unaffected. The FRM method hence allows to distinguish different contributions affecting the SQUID voltage.

Figure 4(a) shows the measured mutual inductance M_{in} of our prototype device as a function of reduced temperature $\tilde{t} = T/T_c^\lambda$. We have performed several static measurements while both, warming up and cooling down, in order to check for potential hysteresis effects that would potentially spoil the detector performance. [14] The FRM measurement was performed with an injected current $I_{\mathrm{in}} = 500\,\mu\mathrm{A}$ and served to affirm the results of the static measurements. The FRM curve can hardly be seen in Fig. 4(a) as it fully overlaps with the data from the static measurements, indicating excellent agreement. We performed an empirical fit of the measured curves using the function

$$fz(\tilde{t}) = M_{\mathrm{in}}^0\{1 - a[1 - z(\tilde{t})]\},$$
$$z(\tilde{t}) = (1 - \tilde{t}^4)^{-1}. \qquad (2)$$

The fit parameter M_{in}^0 describes the mutual inductance at zero temperature, and the constant a quantifies the magnitude of the temperature change of $M_{\mathrm{in}}(T)$. This fit is used for the prediction of noise performance. The overall shape of the curve with the very strong increase in $M_{\mathrm{in}}(T)$ close to T_c^λ arises from the temperature dependence of $\lambda(T)$,
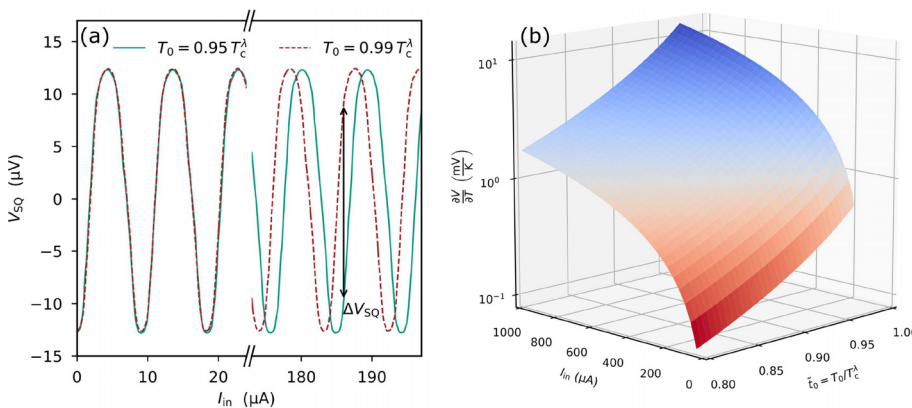

FIG. 3. (a) Output voltage V_{SQ} of our test device vs the input current I_{in} for two different operation temperatures. The change in M_{in} is small, but with a sufficiently large choice of the input current I_{in}, a sizeable signal ΔV_{SQ} can be achieved. (b) Gain coefficient $\partial V_{\mathrm{SQ}}/\partial T$ vs the input current I_{in} and the reduced operation temperature $\tilde{t}_0 = T_0/T_c^\lambda$.
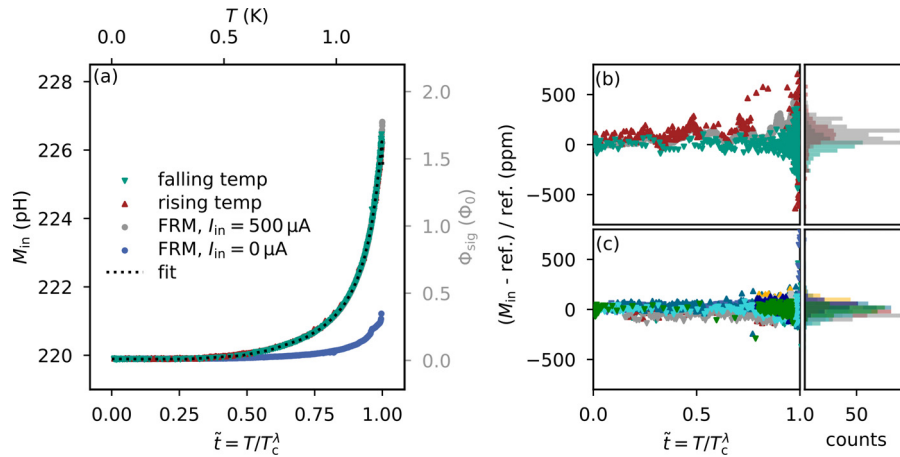
09 April 2025 20:46:20

FIG. 4. (a) Mutual inductance M_{in} (left axis) as a function of reduced temperature $\tilde{t} = T/T_c^\lambda$ for two static measurements (performed with increasing and decreasing temperature, respectively,) as well as an FRM measurement with $I_{in} = 500\,\mu A$. Moreover, an empirical fit to these curves is shown as explained in the main text. Additionally, the signal flux Φ (right axis) is displayed for the FRM measurements. (b) Deviation of the curves for rising temperature (red, ▼), falling temperature (green, ▲), and FRM with $I_{in} = 500\,\mu A$ to a common, smoothed reference curve (ref.) to substantiate the excellent agreement. A histogram of the deviation data is also provided. The mean deviation from 0 is below 250 ppm, indicating that no significant hysteresis is present between measuring during warm-up and cooldown. (c) is equivalent to (b), but for a second test device of identical design. For this device, six curves of $M_{in}(T)$ while cooling down (▼, various colors) and four curves while warming up (▲, various colors) were acquired using the static method. Again, no statistically significant deviation is present.

which diverges at the critical temperature. To illustrate the excellent agreement between the three datasets and hence the absence of any hysteresis effects, their deviation from a common, smoothed reference curve is displayed in Fig. 4(b). The deviation of some data points in the curve for rising temperature (red, ▲) is due to a thermal instability of our cryostat in the temperature range of 800 mK to 1 K, leading to sudden and fast changes in temperature causing an offset between measured and actual temperature of the test device. Over a large temperature range, the deviation between data sets is lower than 250 ppm, as can be seen from the histogram representation. Similarly, a total of ten static measurements were performed on a second, identical test device. Six of these were measured while cooling down, four curves while warming up. Again, their deviations to a smoothed reference curve were determined and are displayed in Fig. 4(c). The related histogram proves again that no statistically relevant offset between warming up and cooling down is present and hence that no hysteresis effects occur.

We additionally performed an FRM measurement without applying an input current to check for parasitic inductance effects [see Fig. 4(a)]. Since $I_{in} = 0$, we cannot use the equation $\Phi(T) = M_{in}(T)I_{in}$ to relate the signal flux Φ to a change in mutual inductance M_{in}. In this scenario, no flux signal is induced via the input coil. Instead, the measured signal is caused by the temperature dependence of the inductance L_λ coupling to the bias current of the SQUID. The parasitic inductance effects are negligible as compared to the change of mutual inductance.

We used the acquired data on $M_{in}(T)$ to estimate the achievable energy resolution ΔE_{FWHM} of a fully equipped microcalorimeter with T_c^λ below 100 mK. For this, we assume that the temperature dependence $M_{in}(\tilde{t})$ solely depends on the reduced temperature $\tilde{t} = T/T_c^\lambda$, i.e.,

$$\frac{dM}{dT} = \frac{\partial M}{\partial \tilde{t}}\frac{d\tilde{t}}{dT}. \tag{3}$$

This assumption is well justified as the magnetic penetration depth of a superconducting material shows this scaling behavior. We hence can use our measured data to extrapolate the energy resolution for a device comprising a superconducting material with lower critical temperature T_c^λ than Al. If the noise of the readout chain reading out the detector is sufficiently low, for example, by using a voltage bias of the detector as well as an N-dc SQUID series array as a first amplifier stage, there are two noise contributions to consider: thermal noise $S_{E,TD}$ resulting from random energy fluctuations among the absorber, sensor, and heat bath as well as SQUID noise $S_{E,SQ}$. The latter is given by

$$S_{E,SQ} = S_{VV}\left(\frac{\partial V_{SQ}}{\partial T}\frac{\partial T}{\partial E}\right)^{-2}, \tag{4}$$

where S_{VV} is the voltage noise of the SQUID, $\partial V_{SQ}/\partial T$ is the gain coefficient, and $1/C_{det} = \partial T/\partial E$ is the inverse total heat capacity. For an optimized dc-SQUID,[10] the SQUID voltage noise can be readily estimated by $S_{VV} = 18k_B TR$. To determine the gain coefficient

$$\frac{\partial V_{SQ}}{\partial T} = \frac{\partial V_{SQ}}{\partial \Phi}\frac{\partial M_{in}}{\partial \tilde{t}}\frac{I_{in}}{T_c^\lambda}, \tag{5}$$

we deduce $\partial M_{in}/\partial \tilde{t}$ from the empirical fit in Fig. 4(a) by evaluating its derivative at the operating temperature T_0. The thermal noise $S_{E,TD}$ among absorber, sensor, and heat bath follows the relation[3,15]

$$S_{E,TD} = k_B C_{sens} T^2\left[\frac{4(1-\beta)\tau_0}{1+(2\pi\tau_0 f)^2} + \frac{4\beta\tau_1}{1+(2\pi\tau_1 f)^2}\right]. \tag{6}$$

Here, τ_0 and τ_1 represent the signal rise and decay time, C_{sens} is the heat capacity of the temperature sensor, and $\beta = C_{sens}/C_{tot}$. The energy resolution ΔE_{FWHM} is then determined by the integral[3,15]

$$\Delta E_{\mathrm{FWHM}} = 2\sqrt{2\ln 2}\left[\int_0^\infty \frac{|p(f)|^2}{S_{\mathrm{E,TD}}(f) + S_{\mathrm{E,SQ}}(f)}\,df\right]^{-1/2}, \quad (7)$$

with the detector responsivity

$$|p(f)| = \frac{2\beta\tau_1}{\sqrt{1 + (2\pi\tau_0 f)^2}\sqrt{1 + (2\pi\tau_1 f)^2}}. \quad (8)$$

For the achievable energy resolution, both noise contributions appear in the denominator of Eq. (7). To calculate the energy resolution caused by only one of these noise contributions as used in the comparison below, only the considered noise appears there.

Figure 5 shows the predicted energy resolution(s) vs the total heat capacity C_{tot} of the detector for three different critical temperatures of the λ-coil. For these calculations, we assumed a conservative input current of $I_{\mathrm{in}} = 500\,\mu\mathrm{A}$, rise and decay times of $\tau_0 = 1\,\mu\mathrm{s}$ and $\tau_1 = 1\,\mathrm{ms}$(Ref. 16) and $\beta = 1/2$ as well as an operating temperature of $T_0 = 0.95T_c^\lambda$. The contributions from SQUID noise (dotted) and thermal noise (dashed) scale differently with the heat capacity, leading to a crossover point below which the thermal noise is dominating. It is worth mentioning that the SQUID noise scales with total heat capacity as the heat capacity and hence the geometric size of the λ-coil must match the absorber heat capacity. As expected, a decrease in T_c^λ (and thus T_0) leads to an overall improvement of the energy resolution as well as a shift of the crossover point toward higher heat capacities. To give a specific example, we want to assume an x-ray detector with a sensitive detection area of $250 \times 250\,\mu\mathrm{m}^2$ and a thickness d of 5, 8.6, and $50\,\mu\mathrm{m}$ for the absorber materials Au, Bi, and Sn, respectively.
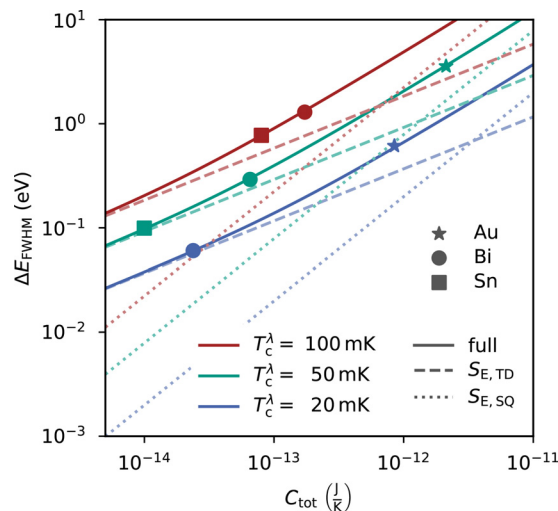

FIG. 5. Predicted energy resolution ΔE_{FWHM} vs total heat capacity C_{tot} of the detector. The achievable energy resolution (solid line) is displayed as well as the effective energy resolutions if we only consider the thermodynamic noise $S_{\mathrm{E,TD}}$ (dashed) or only the noise $S_{\mathrm{E,SQ}}$ of the λ-SQUID (dotted), respectively. Curves for three values of $T_c^\lambda = 100\,\mathrm{mK}$ (red), $T_c^\lambda = 50\,\mathrm{mK}$ (green), and $T_c^\lambda = 20\,\mathrm{mK}$ (blue) at a constant input current of $I_{\mathrm{in}} = 500\,\mu\mathrm{A}$. Stars, circles, and squares mark the full energy resolution when using absorbers made from Au, Bi, and Sn, respectively, at the respective temperatures.

Thus, the stopping power is roughly identical for all materials and exceeds 99.99% at photon energies up to 1 keV. We select gold, bismuth, and tin as absorber material as these materials are often used in the cryogenic microcalorimeter community.[9,17,18] Figure 5 shows that for a proper combination of absorber material and critical temperature of the sensor material, an energy resolution as low as 300 meV should be feasible. It should be mentioned that a Bi absorber operated close to 50 mK with a specific heat of $6.5 \times 10^{-14}\,\mathrm{JK}^{-1}$ would experience a temperature increase in 2.46 mK (or just below 5% of T_c^λ) upon absorption of a 1 keV photon. It is thus expected to display some nonlinear behavior, which may potentially be predicted theoretically and compensated for. Moreover, it should be noted that increasing the input current I_{in} suppresses the SQUID noise contribution further [cf. Eq. (1)]. This allows, for example, to compensate for a potential readout noise degradation when using SQUID-based multiplexing techniques.[19]

In conclusion, we have presented an innovative concept for a SQUID-based superconducting microcalorimeter with an *in situ* tunable gain. It is based on the strong temperature dependence of the magnetic penetration depth of a superconductor close to its critical temperature T_c that affects the mutual inductance M_{in} between the SQUID loop and an input coil that is biased with a constant current. The latter can be easily tuned *in situ*. This allows, for example, for compensating a potential noise degradation when using cryogenic multiplexing techniques. We have designed, fabricated, and characterized a prototype device using aluminum as sensor material to study the temperature dependence of M_{in}. We find that there is no sign for any hysteresis effects that often spoil the performance of superconducting microcalorimeters. Using these data, we have made predictions of the achievable energy resolution. We found that the lower the total specific heat C_{tot} of the detector, the easier it is to suppress the λ-SQUID noise below the thermal noise floor. More specifically, we found that an energy resolution $\mathcal{O}(300\,\mathrm{meV})$ with a suitable combination of absorber and sensor material is possible.

AUTHOR DECLARATIONS
Conflict of Interest

The authors have no conflicts to disclose.

Author Contributions

Constantin Schuster: Conceptualization (equal); Formal analysis (equal); Investigation (lead); Software (lead); Visualization (lead); Writing – original draft (equal); Writing – review & editing (equal). **Sebastian Kempf:** Conceptualization (equal); Formal analysis (equal); Investigation (supporting); Visualization (supporting); Writing – original draft (equal); Writing – review & editing (equal).

09 April 2025 20:46:20

DATA AVAILABILITY

The data that support the findings of this study are available from the corresponding author upon reasonable request.

REFERENCES

[1] G. Irwin and K. D. Hilton, "Transition-edge sensors," in *Cryogenic Particle Detection*, edited by C. Enss (Springer, Berlin, Heidelberg, 2005), pp. 63–150.

[2] J. N. Ullom and D. A. Bennett, "Review of superconducting transition-edge sensors for x-ray and gamma-ray spectroscopy," Supercond. Sci. Technol. **28**, 084003 (2015).

[3] A. Fleischmann, C. Enss, and G. Seidel, "Metallic magnetic calorimeters," in *Cryogenic Particle Detection*, edited by C. Enss (Springer, Berlin, Heidelberg, 2005), pp. 151–216.

[4] S. Kempf, A. Fleischmann, L. Gastaldo, and C. Enss, "Physics and applications of metallic magnetic calorimeters," J. Low Temp. Phys. **193**, 365 (2018).

[5] S. Friedrich, "Cryogenic X-ray detectors for synchrotron science," J. Synchrotron Rad. **13**, 159–171 (2006).

[6] W. B. Doriese, K. M. Morgan, D. A. Bennett, E. V. Denison, C. P. Fitzgerald, J. W. Fowler, J. D. Gard, J. P. Hays-Wehle, G. C. Hilton, K. D. Irwin, Y. I. Joe, J. A. B. Mates, G. C. O'Neil, C. D. Reintsema, N. O. Robbins, D. R. Schmidt, D. S. Swetz, H. Tatsuno, L. R. Vale, and J. N. Ullom, "Developments in time-division multiplexing of x-ray transition-edge sensors," J. Low Temp. Phys. **184**, 389–395 (2016).

[7] J. Uhlig, W. B. Doriese, J. W. Fowler, D. S. Swetz, C. Jaye, D. A. Fischer, C. D. Reintsema, D. A. Bennett, L. R. Vale, U. Mandal, G. C. O'Neil, L. Miaja-Avila, Y. I. Joe, A. El Nahhas, W. Fullagar, F. Parnefjord Gustafsson, V. Sundström, D. Kurunthu, G. C. Hilton, D. R. Schmidt, and J. N. Ullom, "High-resolution X-ray emission spectroscopy with transition-edge sensors: Present performance and future potential," J. Synchrotron Rad. **22**, 766–775 (2015).

[8] S. J. Lee, J. S. Adams, S. R. Bandler, J. A. Chervenak, M. E. Eckart, F. M. Finkbeiner, R. L. Kelley, C. A. Kilbourne, F. S. Porter, J. E. Sadleir, S. J. Smith, and E. J. Wassell, "Fine pitch transition-edge sensor X-ray microcalorimeters with sub-eV energy resolution at 1.5 keV," Appl. Phys. Lett. **107**, 223503 (2015).

[9] M. Krantz, F. Toschi, B. Maier, G. Heine, C. Enss, and S. Kempf, "Magnetic microcalorimeter with paramagnetic temperature sensor and integrated dc-SQUID readout for high-resolution x-ray emission spectroscopy," Appl. Phy. Lett. (submitted).

[10] C. D. Tesche and J. Clarke, "dc SQUID: Noise and optimization," J. Low Temp. Phys. **29**, 301–331 (1977).

[11] D. Drung, C. Hinnrichs, and H.-J. Barthelmess, "Low-noise ultra-high-speed dc SQUID readout electronics," Supercond. Sci. Technol. **19**, S235 (2006).

[12] J. A. Mates, K. D. Irwin, L. R. Vale, G. C. Hilton, J. Gao, and K. W. Lehnert, "Flux-ramp modulation for SQUID multiplexing," J. Low Temp. Phys. **167**, 707–712 (2012).

[13] D. Richter, L. Hoibl, T. Wolber, N. Karcher, A. Fleischmann, C. Enss, M. Weber, O. Sander, and S. Kempf, "Flux ramp modulation based MHz frequency-division dc-SQUID multiplexer," Appl. Phys. Lett. **118**, 122601 (2021).

[14] T. R. Stevenson, M. A. Balvin, S. R. Bandler, S. E. Busch, K. L. Denis, W.-T. Hsieh, D. P. Kelly, W. Merrell, P. C. Nagler, J.-P. Porst, J. E. Sadleir, G. M. Seidel, and S. J. Smith, "Superconducting effects in optimization of magnetic penetration thermometers for x-ray microcalorimeters," IEEE Trans. Appl. Supercond. **23**, 2300605 (2013).

[15] D. McCammon, "Thermal equilibrium calorimeters—An introduction," in *Cryogenic Particle Detection*, edited by C. Enss (Springer, Berlin, Heidelberg, 2005), pp. 1–34.

[16] The rise and decay times can be set via the design of the thermal links between absorber, sensor and thermal bath. As the energy resolution scales like $\Delta E_{FWHM} \propto (\tau_0/\tau_1)^{1/4}$, a reduction of the decay time comes at a cost of increased thermodynamic energy fluctuations.[3] The values used here are typical for MMCs, but can be tuned to suit other applications.

[17] R. D. Horansky, J. N. Ullom, J. A. Beall, G. C. Hilton, K. D. Irwin, D. E. Dry, E. P. Hastings, S. P. Lamont, C. R. Rudy, and M. W. Rabin, "Superconducting calorimetric alpha particle sensors for nuclear nonproliferation applications," Appl. Phys. Lett. **93**, 123504 (2008).

[18] A.-D. Brown, S. R. Bandler, R. Brekosky, J. A. Chervenak, E. Figueroa-Feliciano, F. Finkbeiner, N. Iyomoto, R. L. Kelley, C. A. Kilbourne, F. S. Porter, S. Smith, T. Saab, and J. Sadleir, "Absorber materials for transition-edge sensor x-ray microcalorimeters," J. Low Temp. Phys. **151**, 413–417 (2008).

[19] K. D. Irwin, "Shannon limits for low-temperature detector readout," AIP Conf. Proc. **1185**, 229 (2009).